Polymers **2014**, *6*, 1489-1501; doi:10.3390/polym6051489

OPEN ACCESS

polymers

ISSN 2073-4360

www.mdpi.com/journal/polymers

Article

Modeling the Kinetics of Enhanced Photo-Polymerization under a Collimated and a Reflecting Focused UV Laser

Jui-Teng Lin [1,†], Hsia-Wei Liu [2,†] and Da-Chuan Cheng [3,*]

[1] New Vision Inc., 5F, No. 27, Lane 10, Jiuquan St., Taipei 103, Taiwan; E-Mail: jtlin55@gmail.com

[2] Department of Life Science, Fu Jen Catholic University, New Taipei City 24205, Taiwan; E-Mail: 079336@mail.fju.edu.tw

[3] Department of Biomedical Imaging and Radiological Science, China Medical University, Taichung 404, Taiwan

[†] These authors contributed equally to this work.

[*] Author to whom correspondence should be addressed; E-Mail: dccheng@mail.cmu.edu.tw; Tel.: +886-4-2205-3366 (ext. 7803); Fax: +886-4-2208-4179.

Received: 27 March 2014; in revised form: 1 May 2014 / Accepted: 12 May 2014 / Published: 20 May 2014

Abstract: This study explored the kinetics of ultraviolet (UV) laser photoinitiated polymerization in thick polymer systems to achieve improved polymerization efficiency and uniformity. The modeling system comprised an incident UV laser and its reflecting beam, which was focused by a concave mirror to compensate for the exponential decay in the absorbing medium. The polymerization kinetic equation was numerically solved for the initiator concentration. The crossover time was calculated and compared among single beam, two collimated beam and collimated plus reflecting focused-beam systems. For the single beam case, analytic formulas for the time dependent incident beam is derived and demonstrated by measured data. A theoretical crossover time is defined to analyze the measured data based on the dynamic moduli. Lastly, the polymerization boundary dynamics are illustrated, showing the advantage of the combined two beam system. The numerical results provide useful guidance and a novel means for accelerated uniform photo-polymerization, which cannot be achieved by other means.

Keywords: modeling; polymerization; photoinitiation; UV laser; crossover time

1. Introduction

The kinetics of photoinitiated polymerization have been studied by many researchers analytically, numerically, and experimentally [1–12]. In general, the laser may be absorbed by the photolysis product; therefore, the kinetics of photoinitiated polymerization, especially in thick polymer systems, are difficult to solve analytically, and only numerical results have been reported in previous studies [9–12]. Commercial type-I photoinitiators that produce two radicals following visible photon absorption have limited water solubility and high cell toxicity [1]. A ultraviolet (UV) laser at 365 nm was used for improved polymerization kinetics at lower initiator concentrations [4]. Various kinetic conditions and different photosensitizers are available in recent review papers [13,14].

We have recently developed semi-analytical modeling for photo-polymerization in a thick polymer (up to 10 mm) under a collimated UV laser [15]. In a collimated system, the photo-polymerization is always faster at the entrance and slower at the exit of the absorbing medium. Therefore, thick absorbing media (>1.0 cm) cannot be completely photopolymerized, especially at the bottom portion. To overcome the drawbacks of collimated laser systems and achieve more uniform photo-polymerization throughout the medium, we previously presented a focused single beam laser system [16].

A modeling system with two counter propagating collimated beams has also been studied to achieve faster photo-polymerization [10]. This study will explore a more complex system, in which a collimated incident beam is reflected by a concave mirror to produce a focused backward beam. Our results show that this reflecting focused-beam achieves not only more uniform photo-polymerization but also a shorter procedure compared with that of the collimated two beam system.

We will introduce a modeling system for improved efficiency and uniformity. The system consists of a collimated incident beam and its reflecting beam, which is focused by a concave mirror to compensate for the exponential decay in the absorbing medium. The polymerization kinetic equation was numerically solved for the initiator concentration. For the single beam case, analytic formulas for the time dependent incident beam is derived and demonstrated by measured data. A theoretical crossover time is defined to analyze the measured data based on the dynamic moduli during photopolymerization [4,16,17]. The crossover time was calculated and compared among the various single beam, two collimated-beam and collimated plus focused reflecting-beam systems. The dynamic profiles of the polymerization rate were analyzed for various conditions. Lastly, the polymerization boundary dynamics are illustrated, showing the advantage of the combined two beam system. To the best of our knowledge, this study provides the first presentation of a novel means for accelerated uniform photo-polymerization.

2. Method

2.1. The Model System

As shown in Figure 1, a collimated UV laser beam propagates along the z-direction of the absorbing medium (with a thickness L) containing a UV photoinitiator. The collimated incident beam is reflected by a concave mirror to produce a focused backward beam, which coexists with the incident beam inside the medium. The reflecting focused beam, $I_2(z,t)$, is related to the incident beam, $I_1(z,t)$, at the boundary of the medium as follows (assuming a total reflection):

$$I_2(L-z,t) = I_2(z=L,t)\cdot F(L-z) \tag{1}$$

where $F(z)$ is a focusing function given by [16]:

$$F(L-z) = \left(1-\frac{1-w}{f}(L-z)\right)^{-2}, \text{ for } z<f \tag{2a}$$

$$F(L-z) = \left(w+\frac{1-w}{1-f}(L-z-f)\right)^{-2}, \text{ for } z>f \tag{2b}$$

where w is the ratio between the beam spot size at $z = 0$ and the spot size at the focal point ($z = f$). The value of w, in general, depends on the divergent angle and beam quality of the focused reflecting beam. We will assume $w = 0.2$ for a typical solid-state laser as the UV light source. If a light-emitting diode (LED) is used as the light source, w will be larger (0.4 to 0.6). In Equation (1), the counter propagation of the reflecting beam is defined by the $(L - z)$ factor, where we have defined $z = 0$ as the entrance plan of the incident collimated beam (see Figure 1 below) in our finite element numerical program. It will be shown later that the reflecting focused-beam achieves not only more uniform photo-polymerization but is also 60% faster compared with that of the collimated one beam system. In Equation (1), the incident UV light is a collimated continuous wave (CW) with a flat temporal and spatial profile such that small distortion of the reflecting beam (in temporal and spatial profile) may be neglected.

Figure 1. Schematic of an incident collimated beam and its reflecting focused-beam counter propagating through an absorbing polymer medium with a thickness L.

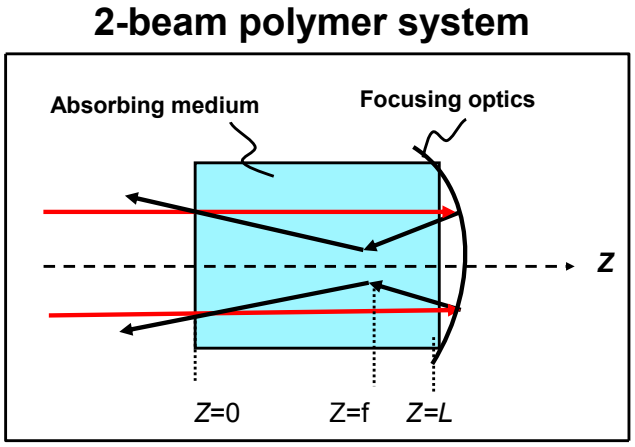

2.2. The Kinetic Equations

The molar concentration of the photoinitiator $C(z,t)$ and the two laser beam intensities $I_j(z,t)$ (with $j = 1, 2$) can be described by a one-dimensional kinetic model [5–9], which is revised in this study to describe a system of two counter propagating beams as follows:

$$\frac{\partial C(z,t)}{\partial t} = -a[I_1(z,t) + I_2(L-z,t)]C(z,t) \tag{3a}$$

$$\frac{\partial I_1(z,t)}{\partial z} = -2.303\left[(\varepsilon_1-\varepsilon_2)C(z,t) + \varepsilon_2 C_0 + A_m\right]I_1(z,t) \tag{3b}$$

$$\frac{\partial I_2(L-z,t)}{\partial z} = -2.303\left[(\varepsilon_1-\varepsilon_2)C(z,t)+\varepsilon_2 C_0 + A_m\right]I_2(L-z,t) \quad (3c)$$

where C_0 is the initial value, $C_0 = C(z,t = 0)$; $a = 83.6\lambda\phi\varepsilon_1$, with ϕ being the quantum yield and λ being the laser wavelength; and ε_1 and ε_2 are the molar extinction coefficients of the initiator and the photolysis product, respectively. A_m is the extinction coefficient of the monomer and the repeat unit. In our calculations, the following units are used: $C(z,t)$ in mM, $I(z,t)$ in (mW/cm^2), λ in cm, z in cm, t in seconds, A_m in (cm)$^{-1}$ and ε_j in (mM·cm)$^{-1}$.

The coupled differential equations were solved, by the finite element method, with the initial and boundary conditions $C(z,0) = C_0$, $I_1(0,t) = I_0$ and $I_2(z = 1.0,t) = I_1(z = 1.0,t)$ for a medium thickness $L = 1.0$ cm. We shall note that the coupled Equation (3) is a highly nonlinear equation, in which the reflecting beam is changing with time due to the time-dependence of the absorption of the incident beam and the initiator concentration. The cross interaction between the incident and the reflecting beam is via their co-propagating in the absorbing medium or their co-coupling to the $C(z,t)$ term shown in Equation (3b) and in Equation (3c). The initiator concentration is depleted in time by both beams as shown by Equation (3a). The counter propagation of the two beams is managed by the $(L - z)$ coordinate for the reflecting beam such that for each pint of time (t) and space (z), the three parameters, $I_1(z,t)$, $I_2(L - z,t)$, $C(z,t)$, are closely coupled and affecting each other. Our numerical simulations require a simultaneous solution of Equation (3) which is much more complex than the single beam situation.

2.3. The Photoinitiation Rate

If two active centers are produced upon defragmentation of the initiator, the local photoinitiation rate for the production of free radicals, $R(z,t)$, is represented by[5]:

$$R(z,t) = 2(83.6\lambda)\varepsilon_1\phi I(z,t)\cdot C(z,t) \quad (4)$$

which is proportional to the product of the light intensity and the initiator concentration. $R(z,t)$ has a unit of mW/cm^3. Example of above two active centers reaction was shown in the experimental study of single beam case using UV light at 365 nm and initiators of 2-hydroxy-1-[4-(2-hydroxyethoxy)phenyl] -2-methyl-1-propanone (I2959) and Lithium pheny1-2,4,6-trimethylbenzoylphosphinate (LAP) [4].

3. Results and Discussion

3.1. Analytical Formulas for the Collimated Beam

For only the incident collimated incident beam without the reflecting beam and when $A_m = \varepsilon_2 = 0$, analytical solutions of Equation (3) are available [5]:

$$C(z,t) = C_0/\left[1+(e^X-1)e^{-Y}\right] \quad (5a)$$

$$I(z,t) = I_0/\left[1+(e^Y-1)e^{-X}\right] \quad (5b)$$

where $X = aI_0t$, $Y = bC_0z$, $a = 83.6\lambda\phi\varepsilon_1$, $b = 2.3\varepsilon_1$.

We define the distance at which the initial normalized light intensity, $I(z = z^*,t)/I_0$ (at $t = 0$), drops to $1/e^2$, or 13.5%, as the penetration depth of the UV light. From Equation (5b) we obtain:

$$z^*(t) = 0.5 z_0 \ln[1 + P(t)] \tag{6}$$

where $P(t) = 6.39 e^{aI_0 t}$, and the initial penetration depth, z*(t = 0), is given by $z_0 = 2/(bC_0)$.

The above equation shows that the penetration depth is inversely proportional to the concentration and the extinction coefficient of the riboflavin solution. It is also a nonlinearly increasing function of the light intensity and irradiation time.

The experimental studies of single beam case using UV light at 365 nm and initiators of I2959 and LAP have been published [4]. However, there is no published experimental work relating to our proposed two beam system. A detailed recent review of the chemical reaction mechanism and experiments of the UV photoinitiation in single beam cases can be also found in references [13,14].

Our analytic formula, Equation (5b), shows that the light intensity is a nonlinearly increasing function of time (t) at a given position (z). To demonstrate this dynamic feature, we measured the light intensity change for a UV light propagating through a riboflavin initiator which was commonly used for the corneal collagen cross linking [16]. Our measured data for the normalized light intensity I/I_0 are shown in Figure 2 for an initial initiator concentration of 0.15% and 0.3% at z = 10 mm, and an initial light intensity of 120 mW/cm^2.

Figure 2. The normalized light intensity I/I_0 *versus* time (t) for initiator riboflavin with an initial concentration of 0.15% (top curve) and 0.3% (lower curve).

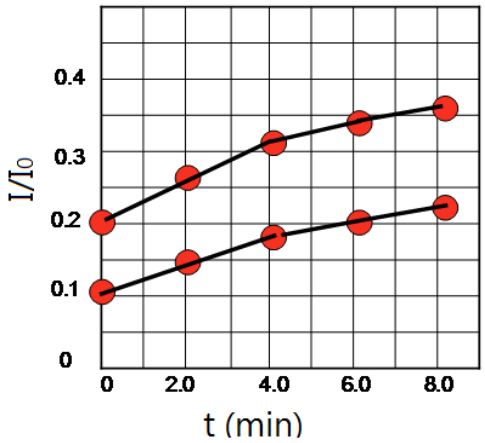

3.2. The Crossover Time

For the single beam collimated case, one may solve Equation (5a) to obtain an analytic formula for the UV light exposure time (t) as a function of the initiator concentration and light intensity as follows:

$$t(z) = 0.5 T_0 \ln(1 + Q') \tag{7a}$$

$$Q'(z) = \left(\frac{C_0}{C(z,t)} - 1 \right) e^{bC_0 z} \tag{7b}$$

$$T_0 = 0.024 / (\varepsilon_1 \phi \lambda I_0) \tag{7c}$$

Experimental crossover time defines the time required to reach the gel point which is defined by the storage-loss moduli of the polymer [4,18–20]. However, a theoretical crossover time (T^*) has not been defined previously. Because the gelation causes the depletion of the initiator concentration and the photoinitiation rate is proportional to the product of the light intensity and the initiator concentration, we propose the possible definition of the crossover time (T^*) shall include: (1) the time required to reach the gel point of the material which needs the measured data of the dynamic moduli and the gel point; (2) the time required for the photoinitiation rate (at a given medium thickness) reaches certain saturated value; or (3) the time required for the initiator concentration $C(z,t = T^*)$ reduces to certain cut-off level such as $1/e$ (0.36) or $1/e^2$ (or 0.135) of its initial value $C(z,0)$.

As defined by Equation (3), the photoinitiation rate, $R(z,t)$, is proportional to the product of the light intensity and the initiator concentration. Therefore, a theoretical T^* based on the depletion level of $C(z,t)$ is equivalent to that of $R(z,t)$. In this study, without knowing the measured moduli, we propose a theoretical T^* based on the depletion cut-off level of the initiator concentration and choose the $1/e^2$ reduction level, or when $C_0/C(z,T^*) = e^2 = 7.39$. Using this definition, an analytical expression for T^* is derived from Equation (7)

$$T^*(z) = 0.5T_0 \ln(1+Q) \tag{8a}$$

$$Q(z) = 6.39e^{2.3\varepsilon_1 C_0 z} \tag{8b}$$

where the surface crossover time $T_0 = T^*(z = 0)$ is given by $T_0 = 0.024/(\varepsilon_1\phi\lambda I_0)$. The above equation shows that the crossover time is a nonlinearly increasing function of z. For a UV laser at 365 nm and for a quantum yield $\phi = 0.2$, $T_0 = 3278/(\varepsilon_1 I_0)$. For example, for $\varepsilon_1 = 0.5$ $(\text{mM}\cdot\text{cm})^{-1}$, $T_s^* = 655$ s for a light intensity $I_0 = 10$ mW/cm^2 and reduces to 218 s for $I_0 = 30$ mW/cm^2. Inside the medium ($z > 0$), the cross over time increases with z, as shown by the Q term of Equation (8b). For example, for $C_0 = 10$ mM (or 0.4% mg/mL) and $I_0 = 10$ mW/cm^2, T^*(at $z = 500$ μm) =825 s, which is 1.26 times of the surface value.

The above described crossover time defined by the depletion cut-off level of the initiator concentration may also be realized as the light exposure time which defines the initiator concentration cut-off level to move from the medium surface ($z = 0$) to the medium thickness ($z = L$). Alternatively, we may define the crossover time by the photoinitiation rate. Using the analytic formula of Equation (5) to calculate $R(z,t)$ defined by Equation (4), we obtain:

$$R(z,t) = \frac{167.2\lambda\phi(\varepsilon_1 C_0 I_0)}{\left[1+(e^Y-1)e^{-X}\right]\left[1+(e^X-1)e^{-Y}\right]} \tag{9}$$

We should note that the photoinitiation rate $R(z,t)$ is characterized by the competing process between $I(z,t)$ and $C(z,t)$. Therefore, we expect an optimal photoinitiation rate defined by both z and t. Taking $\partial R(z,t)/\partial(\varepsilon_1 C_0) = 0$ at $C(z,t) = C_0^*$, we may derive an optimal product ($\varepsilon_1 C_0^*$) which is proportional to e^X/z. More detail of the optimal photoinitiation rate will be published elsewhere [17].

Our theoretical T^* may be used to analyze the measured crossover time of reference [4] which showed that the crossover time is inversely proportional to the UV light intensity. These measured features are consistent with our formula Equation (8a). However, unlike our theoretical T^* (with z-dependent), their data only showed the crossover time for the completion of gelation for a given thickness (z) and did not measure the z-dependence of T^*. Our theory provides useful guidance for

future experimental works. The measured crossover time of reference [4] may be also analyzed by Equation (9) as follows. For a given cut-off level of the photoinitiation rate $R^*(z,T^*)$, the crossover time is inverse proportional to R^* and is found to be proportional to $\varepsilon_1 C_0 I_0$ from Equation (9) [17]. Furthermore, higher photoinitiation rate provides a shorter crossover time for gelation. This relationship is consistent with the measured data of reference [4], where the crossover time is a decreasing function of the light intensity and the initiator initial concentration.

3.3. Numerical Results

For an incident beam with a reflecting focus beam, Equation (3) requires numerical simulations. Using the finite element method and program for both the forward and backward beams, we solved for various cases: (a) incident collimated beam only; (b) incident beam with reflecting collimated beam; and (c) incident beam with reflecting focused-beam. In our calculations, we used typical values as follows. For UV light at 365 nm, $\lambda = 3.65 \times 10^{-5}$, we find $83.6\lambda = 0.00305$ and $a = 0.0006\varepsilon_1$ for $\phi = 0.2$. Other parameters used are as follows: light intensity $I_0 = 100$ (mW/cm^2), $C_0 = 10$ mM, $\varepsilon_1 = 0.25$ (mM·cm)$^{-1}$, $\varepsilon_2 = 0.05$ (mM·cm)$^{-1}$ and $A_m = 0$.

Figure 3 shows profiles of the normalized initiator concentration, $C(z,t)/C_0$, *versus* the polymer thickness (z) at t = 17 s (left figure) and 24 s (right figure) for the above 3 cases. As we expect, comparing to the collimated cases, case (c) starts crossover earlier (at t = 7 s) from z = 0.5 (at its focusing position, f = 0.5 cm), whereas cases (a) and (b) start at t = 24 s (z = 0). At t = 24 s, case (c) has completed the crossover central range between z = 0.42 and z = 0.58 cm. In addition, all three cases have the same crossover point at z = 0 which has very weak reflecting beam intensity. The red straight line in Figure 3 represents $1/e^2$ =0.135, which defines the crossover time by its cross points with the profiles of $C(z,t)$.

Figure 3. Profiles of the normalized initiator concentration *versus* the polymer thickness (z) at t = 17 and 24 s for various cases: (a) (solid curve) collimated beam without the reflecting beam; (b) (dashed curve) collimated beam with a collimated reflecting beam, and (c) (dotted curve) collimated beam with a focused reflecting beam.

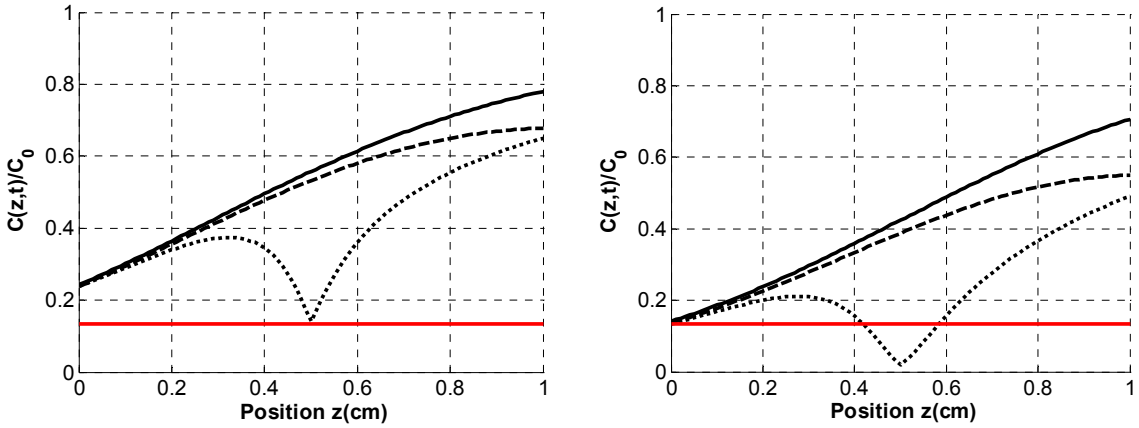

t = 17 s t = 24 s

Figure 4 shows the dynamic profiles of $C(z,t)/C_0$ *versus* z at various times for case (a), an incident collimated beam without a reflecting beam, in which the cross points between the 0.135 straight-line and the curves define the crossover times (T^*) at various z. These cross point provide us the information including: (a) location and when the crossover starts and ends; (b) how long the crossover takes; and (c) time required for the crossover to complete the whole thickness (at $z = L$ =1.0 cm). All of the $C(z,t)/C_0$ curves have the lowest values at z = 0 and highest value at z = 1.0 cm, indicating that the crossover always starts from the entrance (z = 0) and ends at the medium thickness ($z = L$). Figure 4 also shows that the crossover procedure takes 46 s to complete, calculated from the difference between T^* = 70 s (for $z = L$) and T^* = 24 s (for z = 0). Comparing Figures 4 and 5, we find that case (b) with reflecting beam completes the crossover earlier than case (a). For example, $T^*(z$ = 1.0 cm) = 50 s for case (b) which is abut 30% faster than case (a) with $T^*(z$ = 1.0 cm) = 70 s. Furthermore, the crossover procedure takes only 50 − 24 = 26 s in the reflecting beam case *versus* 46 s in the single beam case. This enhancement may be explained by the fact that with the same incident light intensity, the reflecting beam contributes additional light intensity and accelerates the crossover process.

Figure 4. Profiles of the normalized initiator concentration *versus* z at t = 15, 24, 35, 50, and 70 s (curves No. 1 to 5) for case (a), an incident collimated beam without a reflecting beam, in which the cross points define the crossover time at z = 0 to 1.0 cm.

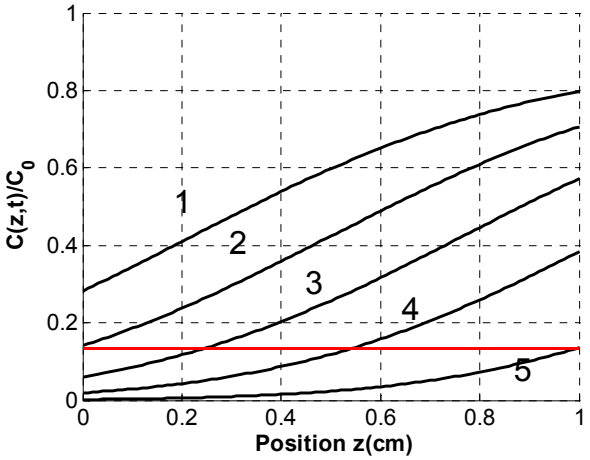

Figure 5. Same as Figure 4, but for case (b), an incident collimated beam with a collimated reflecting beam at t = 15, 24, 30, 35, 40, and 50 s (curves No. 1 to 7).

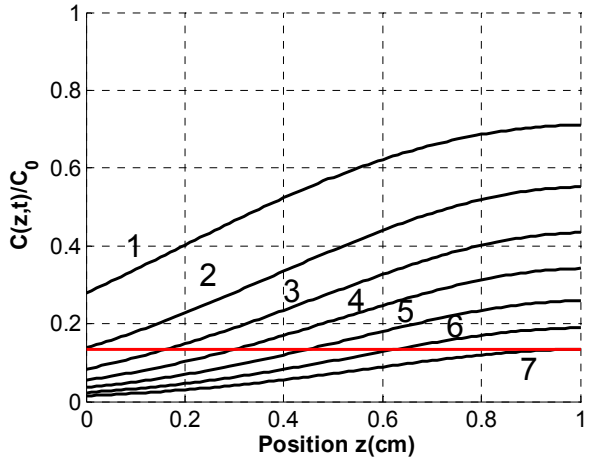

Figure 6 shows that the focal length for $f = 0.75$ cm has faster crossover at the back portion of the medium ($z > 0.5$ cm) than the $f = 0.5$ cm case, which has faster crossover at the front portion ($z < 0.5$ cm). That is, the crossover always starts from the focal point of the laser inside the medium that has the highest laser intensity (or power density). The case with $f = 0.75$ cm is a longer crossover procedure 42 − 13.8 = 28 s than that of $f = 0.5$ cm (27 s). However, it is has a shorter crossover time having $T^* = 42$ s *versus* 44 s at $z = 0.0$ cm.

Figure 6. Same as Figure 4, but for case (c), an incident collimated beam with a focused reflecting beam with a focal length $f = 0.5$ cm (**A**) at t =15, 17, 24, 29, 35, and 44 s for curves No. 1 to 7 and $f = 0.75$ cm (**B**) at $t = 13.8$, 18.8, 23.3, 30, 35, and 42 s for curves No. 1 to 6.

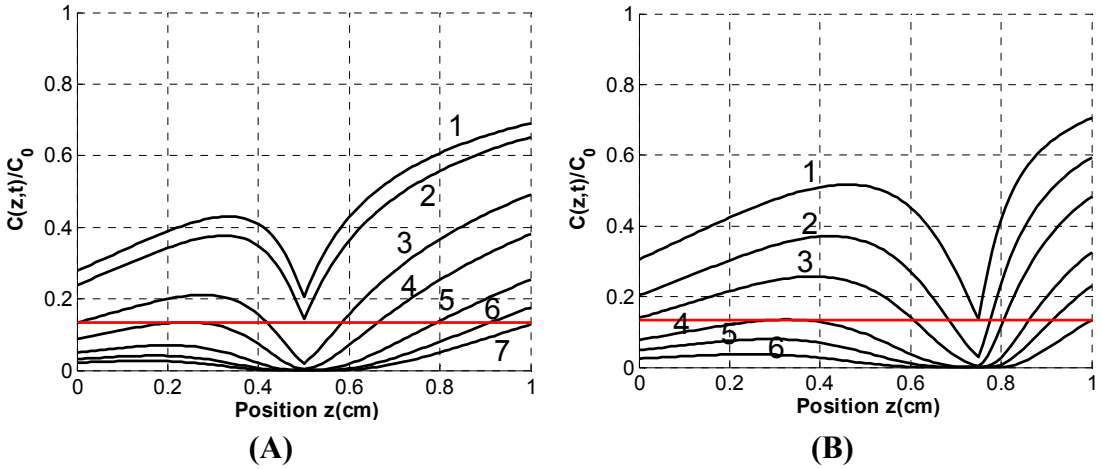

3.4. The Kinetic Rate Function

By numerical simulation, we solve the coupled kinetic Equation (3) and calculate the rate function defined by Equation (4). Figure 7 shows the dynamics of the reduced rate function defined by $R(z,t)/R_0$, with $R_0 = 83.6\lambda$ at $t = 17$ s, for the 3 cases: (a) solid curve; (b) dashed curve; and (c) dotted curves. We note that the crossover rate function has a maximum at about $z = 0.3$ cm and a much lower vale at the output end (at $z = 1.0$ cm) which is enhanced by the reflecting beam as shown by the dashed and dotted curves in Figure 7. Furthermore, the dip shown in the focused case (dotted curve) demonstrates that the crossover starts from the focal point of the reflecting beam at $z = 0.5$ cm. This feature is also illustrated by the initiator depletion shown in Figure 6.

3.5. The Crossover Time

Figure 8 shows the crossover times $T^*(z)$ calculated by the crossing points of the constant line $z = 0.135$ and the profile curves of $C(z,t)/C_0$ shown in Figures 4–6, respectively, for case (a) collimated single beam (cubic); (b) collimated two beam (triangles); and (c) collimated plus focused beam (circles). As we expect that case (a) has the largest T^* (or slowest crossover procedure); case (b) is faster than case (a) due to the extra laser intensity of the reflecting collimated beam. The crossover is further accelerated by the focusing mirror in case (c). The gelation completion time, defined by $T^*(z = 1.0$ cm), was found to be 70, 50 and 44 s for case (a), (b) and (c), respectively. These data

demonstrate that case (c) is about 60% faster than case (a). As shown by our analytical formulas in Equation (7), the crossover time $T^*(z)$ for the collimated cases (a) and (b) is an increasing function of z. The nonlinear curve of case (c) is due to the focusing function shown by Equation (2).

Figure 7. The reduced rate function R *versus* z at t = 17 s for case (a) single beam (dashed curve); case (b), two collimated beams (solid curve); and case (c), a collimated and a focused beam (dotted curves).

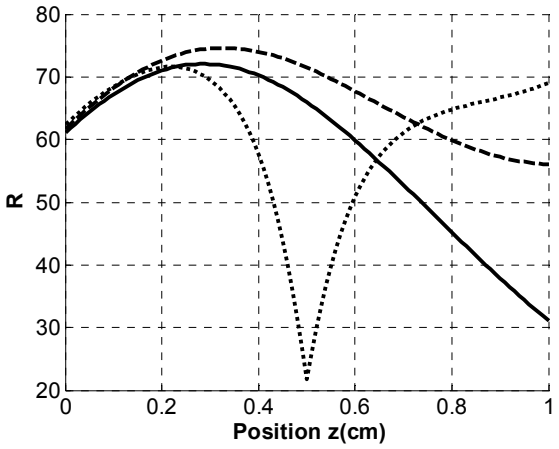

Figure 8. The crossover time associate with Figures 3–5 for a collimated single beam (cubic); two collimated beams (triangles); and a collimated plus a focused beam (circles).

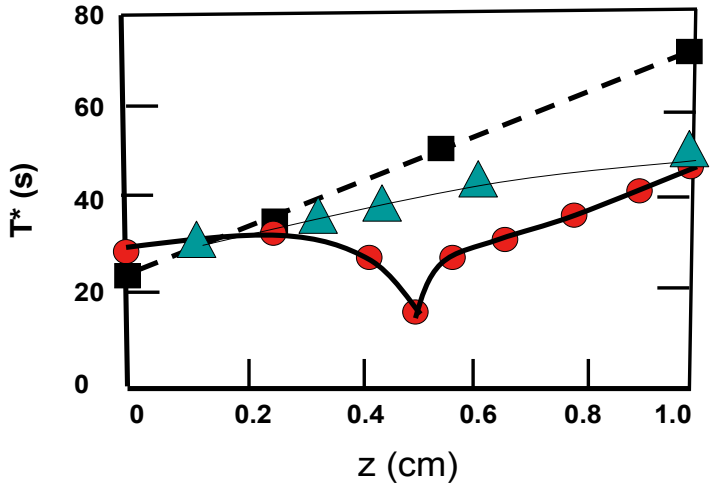

The crossover process is further illustrated by the crossover boundary shown in Figure 9, which also shows the faster crossover at the back portion of the medium (z > 0.5 cm) compared with that at the front portion (z < 0.5 cm) of the medium for the focused case (also shown by Figure 6.) That is, the crossover always starts from the focal point of the laser inside the medium that has the highest laser intensity (power density). The disadvantage of the focused case is that the crossover area (volume) is reduced to the focusing range. This drawback could be overcome by a scanning technique in which the laser beam is scanned along the direction normal to z to cover a wider polymerization area (volume) inside the medium. A 3-dimensional simulation (under progress) is needed to show the profiles. In comparison with the two beam focused case shown in Figure 9, we also show our previously

published single beam focused case (without reflecting beam) [16] in Figure 10, in which the crossover area is larger than the two-beam case. However, the two-beam cases (b) and (c) show faster polymerization than the single beam case (without the reflecting beam) due to the extra laser power from the reflecting beam.

Figure 9. Schematics of the time evolution (from 25 to 40 s) of photo-polymerization for: (**top**) a collimated beam without a reflecting beam; and (**bottom**) a collimated beam with a reflecting focused beam (with $f = 0.5\ L$), where the polymerized portions are shown by shaded areas.

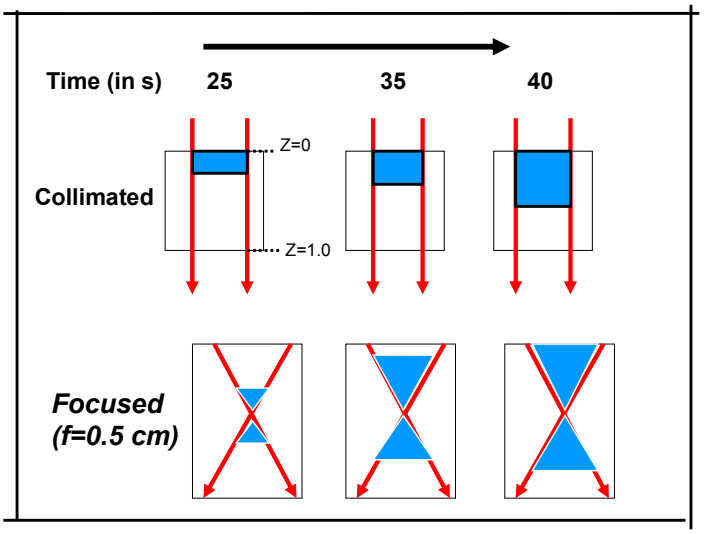

Figure 10. Schematics of the time evolution (from 25 to 40 s) of photo-polymerization for the single beam system (without reflection) under various focusing conditions: (**1**) collimated; (**2**) tightly focusing; (**3**) optimal focusing; and (**4**) slightly focusing [16].

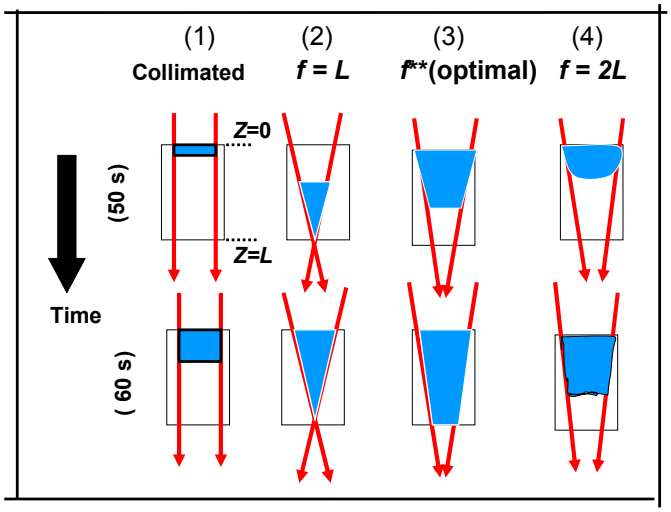

4. Conclusions

We have presented a comprehensive model of the kinetics of photoinitiated polymerization using a UV laser in thick polymer systems. For only a collimated incident beam without a reflecting beam, the analytical formulas are represented by Equations (6) and (7), which allows us to analyze the

penetration depth and crossover time. As shown in Figure 1, the reflecting focused-beam is proposed to compensate for the exponential decay in the absorbing medium. The polymerization boundary dynamics are illustrated in Figure 9, showing the advantage of the reflecting beam system, which achieves not only more uniform photo-polymerization but also a faster procedure (shown by Figure 8). The kinetic equations are numerically solved for the initiator concentration, as shown by Figure 6. The crossover time was calculated and compared among the various single beams, two collimated beams, and collimated plus focused reflecting-beam systems. Our numerical results provide useful guidance and a novel mean for fast and highly efficient photo-polymerization in thick medium.

Acknowledgments

The authors are grateful for financial support from the National Science Council, NSC 102-2221-E-039-005 and NSC 102-2221-E-030-002. This work was also partially supported by a grant from the Xiamen-200 program (Xiamen Science & Technology Bureau, China).

Author Contributions

J.T. Lin initiated the system, derived the formulas and wrote the first draft of the manuscript. H.W. Liu provided the laboratory facilities and developed the measured data shown in Figure 2. D.C. Cheng developed the computer codes and generated all the data shown in the manuscript. J.T. Lin and D.C. Cheng also involved the final version of the manuscript.

Conflicts of Interest

The authors declare no conflict of interest.

References

1. Bryant, S.J.; Nuttelman, C.R.; Anseth, K.S. Cytocompatibility of UV and visible light photoinitiating systems on cultured NIH/3T3 fibroblasts *in vitro*. *J. Biomater. Sci. Polym. Ed.* **2000**, *11*, 439–457.
2. Fouassier, J.-P. *Photoinitiation, Photo-polymerization, and Photocuring: Fundamentals and Applications*; Hanser Gardner Publications: Munich, Germany, 1995.
3. Odian, G. *Principles of Polymerization*; Wiley: New York, NY, USA, 1991.
4. Fairbanks, B.D.; Schwartz, M.P.; Bowman, C.N.; Anseth, K.S. Photoinitiated polymerization of PEG-diacrylate with lithium phenyl-2,4,6-trimethylbenzoylphosphinate: Polymerization rate and cytocompatibility. *Biomaterials* **2009**, *30*, 6702–6707.
5. Terrones, G.; Pearlstein, A.J. Effects of optical attenuation and consumption of a photobleaching initiator on local initiation rates in photopolymerizations. *Macromolecules* **2001**, *34*, 3195–3204.
6. Terrones, G.; Pearlstein, A.J. Effects of kinetics and optical attenuation on the completeness and uniformity of monomer conversion in free-radical photo-polymerizations. *Macromolecules* **2001**, *34*, 8894–8906.
7. Terrones, G.; Pearlstein, A.J. Nonuniformity of chain-length distributions in photopolymerized layers. *Macromolecules* **2003**, *36*, 6346–6358.

8. Ivanov, V.V.; Decker, C. Kinetic study of photoinitiated frontal polymerization. *Polym. Int.* **2001**, *50*, 113–118.
9. Miller, G.A.; Gou, L.; Narayanan, V.; Scranton, A.B. Modeling of photobleaching for the photoinitiation of thick polymerization systems. *J. Polym. Sci. A Polym. Chem.* **2002**, *40*, 793–808.
10. Kenning, N.S.; Kriks, D.; El-Maazawi, M.; Scranton, A. Spatial and temporal evolution of the photo initiation rate for thick polymer systems illuminated on both sides. *Polym. Int.* **2005**, *54*, 1429–1439.
11. Kenning, N.S.; Kriks, D.; El-Maazawi, M.; Scranton, A. Spatial and temporal evolution of the photoinitiation rate for thick polymer systems illuminated with polychromatic light. *Polym. Int.* **2006**, *55*, 994–1006.
12. Kenning, N.S.; Ficek, B.A.; Hoppe, C.C.; Scranton, A.B. Spatial and temporal evolution of the photoinitiation rate for thick polymer systems illuminated by polychromatic light: Selection of efficient photoinitiators for LED or mercury lamps. *Polym. Int.* **2009**, *58*, 1134–1140.
13. Qi, Y.; Gleeson, M.R.; Guo, J.; Callego, S.; Sheridan, J.T. Quantitative comparison of five different photosensitizers for use in a photopolymers. *Phys. Res. Int.* **2012**, 975948:1–975948:11.
14. Guo, J.; Gleeson, M.R.; Sheridan, J.T. A review of the optimisation of photopolymer materials for holographic data storage system techniques. *Phys. Res. Int.* **2012**, 803439:1–803439:16.
15. Lin, J.T.; Huang, D.W.; Cheng, D.C. Modeling the dynamics and optimal photoinitiation rate in thick polymer systems illuminated by a UV light. *Macromol. Theory Simul.* **2014**, submitted.
16. Lin, J.T.; Cheng, D.C. Optimal focusing and scaling law for uniform photo-polymerization in a thick medium using a focused UV Laser. *Polymers* **2014**, *6*, 552–564.
17. Lin, J.T. Analysis on the critical issues of UV light induced corneal cross linking. *Int. J. Latest Res. Eng. Comput.* **2013**, *1*, 104–110.
18. Cruise, G.M.; Scharp, D.S.; Hubbell, J.A. Characterization of permeability and network structure of interfacially photopolymerized poly(ethyleneglycol) diacrylate hydrogels. *Biomaterials* **1998**, *19*, 1287–1294.
19. Chiou, B.S.; English, R.J.; Khan, S.A. Rheology and photo-cross-linking of thiol-ene polymers. *Macromolecules* **1996**, *29*, 5368–5374.
20. Winter, H.H. Can the gel point of a cross-linking polymer be detected by the G'–G'' crossover. *Polym. Eng. Sci.* **1987**, 27, 1698–1702.